J|A|C|S
ARTICLES
Published on Web 11/19/2004

Electronic Structure and Chemical Bonding in MO_n^- and MO_n Clusters (M = Mo, W; n = 3−5): A Photoelectron Spectroscopy and ab Initio Study

Hua-Jin Zhai,[†,‡] Boggavarapu Kiran,[†,‡] Li-Feng Cui,[†,‡] Xi Li,[†,‡] David A. Dixon,[§] and Lai-Sheng Wang*[,†,‡]

Contribution from the Department of Physics, Washington State University, 2710 University Drive, Richland, Washington 99352, W. R. Wiley Environmental Molecular Sciences Laboratory, Pacific Northwest National Laboratory, MS K8-88, P.O. Box 999, Richland, Washington 99352, and Department of Chemistry, University of Alabama, Tuscaloosa, Alabama 35487-0336

Received June 11, 2004; E-mail: ls.wang@pnl.gov

Abstract: Photoelectron spectroscopy (PES) and ab initio calculations are combined to investigate the electronic structure of MO_n^- clusters (M = W, Mo; n = 3−5). Similar PES spectra were observed between the W and Mo species. A large energy gap between the first and second PES bands was observed for MO_3^- and correlated with a stable closed-shell MO_3 neutral cluster. The electron binding energies of MO_4^- increase significantly relative to those of MO_3^-, and there is also an abrupt spectral pattern change between MO_3^- and MO_4^-. Both MO_4^- and MO_5^- give PES features with extremely high electron binding energies (>5.0 eV) due to oxygen-2p-based orbitals. The experimental results are compared with extensive density functional and ab initio [CCSD(T)] calculations, which were performed to elucidate the electronic and structural evolution for the tungsten oxide clusters. WO_3 is found to be a closed-shell, nonplanar molecule with C_{3v} symmetry. WO_4 is shown to have a triplet ground state ($^3A_2$) with D_{2d} symmetry, whereas WO_5 is found to be an unusual charge-transfer complex, $(O_2^-)WO_3^+$. WO_4 and WO_5 are shown to possess W−O$^\bullet$ and $O_2^{-\bullet}$ radical characters, respectively.

Introduction

Transition-metal oxides are widely used in important industrial processes, both as catalysts and as catalytic supports. In particular, the catalytic activity of tungsten oxides[1−6] and molybdenum oxides[7−9] have been extensively studied. The identification of active sites in transition-metal oxide catalysts is difficult and, due to their extreme complexity, often leads to differing hypotheses as to the molecular mode of action. As a first step in developing a comprehensive understanding of complex catalytic processes on transition-metal oxides, we are studying the structure and reactivity of isolated transition-metal oxide clusters. Gas-phase studies, coupled with reliable theoretical calculations, can provide powerful insight into the nature of active species in catalysis at the molecular level.[10,11]

We are interested in probing the electronic structure of transition-metal oxide clusters aiming at providing molecular models and mechanistic insight for the oxide catalysts as well as providing experimental data for the benchmark of theoretical methods.[12−18] Among our previous works is a study on a series of CrO_n and CrO_n^- clusters.[17] In the present work, we investigate the electronic structure and chemical bonding of the heavier group VI MO_n and MO_n^- species (M = W, Mo; n = 3−5), using anion photoelectron spectroscopy (PES) and ab initio and density functional theory (DFT) calculations.

For the mono-tungsten oxide clusters, high-resolution spectroscopic data are available for WO,[19−25] WO_2,[23] and WO_2^-.[24]

[†] Washington State University.
[‡] Pacific Northwest National Laboratory.
[§] University of Alabama.

(1) Katrib, A.; Mey, D.; Maire, G. *Catal. Today* **2001**, *65*, 179.
(2) Baertsch, C. D.; Soled, S. L.; Iglesia, E. *J. Phys. Chem. B* **2001**, *105*, 1320.
(3) Li, S.; Xiao, T.; Li, S.; Chou, L.; Zhang, B.; Xu, C.; Hou, R.; York, A. P. E.; Green, M. L. H. *J. Catal.* **2003**, *220*, 47.
(4) Hilbrig, F.; Gobel, H. E.; Knozinger, H.; Schmelz, H.; Lengeler, B. *J. Phys. Chem.* **1991**, *95*, 6973.
(5) Benitez, V. M.; Figoli, N. S. *Catal. Commun*. **2002**, *3*, 487.
(6) Martin, C.; Solana, G.; Malet, P.; Rives, V. *Catal. Today* **2003**, *78*, 365.
(7) Seman, M.; Kondo, J. N.; Domen, K.; Reed, C.; Oyama, S. T. *J. Phys. Chem. B* **2004**, *108*, 3231.
(8) Liu, H.; Cheung, P.; Iglesia, E. *J. Phys. Chem. B* **2003**, *107*, 4118.
(9) Okamoto, Y.; Oshima, N.; Kobayashi, Y.; Terasaki, O.; Kodaira, T.; Kubota, T. *Phys. Chem. Chem. Phys.* **2002**, *4*, 2852.
(10) Fialko, E. F.; Kirkhtenko, A. V.; Goncharov, V. B.; Zamaraev, K. I. *J. Phys. Chem. B* **1997**, *101*, 5772.
(11) Waters, T.; O'hair, R. A.; Wedd, A. G. *J. Am. Chem. Soc*. **2003**, *125*, 3384.
(12) Wu, H.; Desai, S. R.; Wang, L. S. *J. Am. Chem. Soc*. **1996**, *118*, 5296.
(13) Wang, L. S.; Wu, H.; Desai, S. R. *Phys. Rev. Lett*. **1996**, *76*, 4853.
(14) Wang, L. S.; Wu, H.; Desai, S. R.; Lou, L. *Phys. Rev. B* **1996**, *53*, 8028.
(15) Wu, H.; Wang, L. S. *J. Chem. Phys*. **1997**, *107*, 8221.
(16) Wang, L. S. Photodetachment Photoelectron Spectroscopy of Transition Metal Oxide Species. In *Photoionization and Photodetachment*; Ng, C. Y., Ed.; Advanced Series in Physical Chemistry Vol. 10; World Scientific: Singapore, 2000; pp 854−957
(17) Gustev, G. L.; Jena, P.; Zhai, H. J.; Wang, L. S. *J. Chem. Phys*. **2001**, *115*, 7935.
(18) Zhai, H. J.; Wang, L. S. *J. Chem. Phys*. **2002**, *117*, 7882.
(19) Gatterer, A.; Krishnamurty, S. G. *Nature* **1952**, *169*, 543.
(20) Weltner, W.; McLeod, D. *J. Mol. Spectrosc.* **1965**, *17*, 276.
(21) Green, D. W.; Ervin, K. M. *J. Mol. Spectrosc*. **1981**, *89*, 145.
(22) Kraus, D.; Saykally, R. J.; Bondybey, V. E. *Chem. Phys. Lett.* **1998**, *295*, 285.
(23) Lorenz, M.; Bondybey, V. E. *Chem. Phys*. **1999**, *241*, 127.

10.1021/ja046536s CCC: $27.50

A vibrationally resolved photoelectron spectrum has been reported for WO_2^-.[26] The electron affinity of the molecule WO_3 has been measured using different methods with a wide spread of values (3.33−3.94 eV).[27−31] Very recently, Stolocic, Kim, and Gantefor (SKG) reported photoelectron spectra of WO_3^- and WO_4^- showing a dramatic decrease of electron binding energies from WO_3^- to WO_4^- and suggested a transition from "atomic-to-molecular adsorption of oxygen" from WO_3^- to WO_4^-.[32] This observation was surprising and in contrast to that from our previously reported CrO_n^- series, where a dramatic increase in electron binding energies was observed from CrO_3^- to CrO_4^-.[17] Previous gas-phase studies on mono-molybdenum oxide clusters include photoelectron spectroscopy of MoO^- and reactions of MoO^+ and MoO_2^+ with CO and CO_2[33,34] as well as infrared spectroscopy of MoO_2, MoO_2^-, and MoO_3 in a neon matrix.[24]

The current study represents a continuation of our research interest in oxide clusters.[12−18] We combined PES data with extensive theoretical calculations to completely elucidate the structures and bonding in the mono-tungsten oxide clusters, WO_n^- and WO_n ($n = 3-5$). The present photoelectron spectrum of WO_4^- is very different from that presented by SKG: we did observe a dramatic increase in electron binding energies from WO_3^- to WO_4^-, similar to the CrO_n^- series.[17] In particular, we found that the ground states of WO_4 and WO_5 clusters are interesting radical species with unpaired electrons, which may be important in developing models for the catalytic activity and selectivity of tungsten oxide catalysts.

Experimental Section

Experimental Method. The experiments were carried out using a magnetic-bottle-type PES apparatus equipped with a laser vaporization supersonic cluster source, details of which have been described previously.[35] Briefly, the MO_n^- cluster anions (M = W, Mo) were produced by laser vaporization of a pure metal target in the presence of a helium carrier gas seeded with 0.5% O_2. Various $M_mO_n^-$ clusters were produced from the source and analyzed using a time-of-flight mass spectrometer. The MO_n^- ($n = 3-5$) species of interest were each mass-selected and decelerated before being photodetached. Two detachment photon energies were used in the current study: 266 (4.661 eV) and 193 nm (6.424 eV). Photoelectrons were collected at nearly 100% efficiency by the magnetic bottle and analyzed in a 3.5 m long electron flight tube. The photoelectron spectra were calibrated using the known spectrum of Cu^-, and the resolution of the apparatus was $\Delta Ek/Ek \approx$ 2.5%, that is, ∼25 meV for 1 eV electrons.

Theoretical Methods. Both density functional theory (DFT) and molecular orbital (MO) theory were used in the current study. We used the Stuttgart quasi-relativistic pseudo-potentials and basis sets[36] augmented with two f-type and one g-type polarization functions (0.256, 0.825, and 0.627) for tungsten as recommended by Martin and Sundermann[37] and the cc-pVTZ basis set for oxygen[38] for the DFT calculations. Two basis sets were used for the MO calculations: (1) an approximate aug-cc-pVDZ basis set consisting of the Stuttgart quasi-relativistic pseudo-potentials and basis sets for W with the aug-cc-pVDZ basis on O[39] and (2) an approximate aug-cc-pVTZ basis set consisting of the Stuttgart quasi-relativistic pseudo-potentials augmented with the 2f and 1g functions for W with the aug-cc-pVTZ basis on O.

We tested a variety of exchange-correlation functionals for accuracy and consistency. All of the calculations are spin-restricted for closed-shell molecules and spin-unrestricted for open-shell species. We found that the predicted structures and properties had a strong dependence on the functional. The B3LYP[40] and BPW91[41] functionals gave artificial-symmetry breaking solutions (low-symmetry minima) for WO_4, whereas the PW91xPW91c[41b,42] functional yielded symmetrical geometries. The calculations on the oxygen-rich species WO_5 resulted in two different electronic states dependent on the functional. Whereas B3LYP and PW91xPW91c converged to a charge-transfer (CT) complex, the BPW91 functional resulted in non-CT minima. Although, in general, DFT methods are less prone to symmetry breaking as compared to UHF,[43] not all DFT functionals show similar behavior. It has previously been noted that the nature of the exchange functional, especially those with some percentage of Hartree−Fock exchange, is more important than the correlation functional in determining the amount of symmetry breaking.[43a] Therefore, it is anticipated that B3LYP may give symmetry-breaking solutions in some cases. However, as described below, B3LYP gives superior results in terms of energies when directly compared to experimental results. Symmetry breaking problems near equilibrium are mainly due to the lack of adequate nondynamical correlation (due to near degenerate valence-bond structures) being included by the method and are not important for most of the species studied here. Therefore, we used the results with the B3LYP functional for our direct comparison with experiment. Harmonic frequency calculations were done to verify that the stationary points are minima. Vertical detachment energies (VDEs) for WO_3^- were calculated using the TD-DFT method.[44] For WO_4^- and WO_5^-, VDEs were calculated using the generalized Koopman's theorem[45] by adding a correction term to the eigenvalues of the anions. The correction term was estimated by eq 1

$$\delta E = E_1 - E_2 - \epsilon_{\mathrm{HOMO}} \tag{1}$$

where δE is the correction term, E_1 and E_2 are the total energies of the anion and neutral in their ground states at the anion equilibrium geometry, and finally ϵ_{HOMO} corresponds to the eigenvalue of the highest

(24) Zhou, M. F.; Andrews, L. *J. Chem. Phys.* **1999**, *111*, 4230.
(25) Ram, R. S.; Lievin, J.; Li, G.; Hirao, T.; Bernath, P. F. *Chem. Phys. Lett.* **2001**, *343*, 437.
(26) Davico, G. E.; Schwartz, R. L.; Ramond, T. M.; Lineberger, W. C. *J. Phys. Chem. A* **1999**, *103*, 6167.
(27) Jensen, D. E.; Miller, W. J. *J. Chem. Phys.* **1970**, *53*, 3287.
(28) Center, R. E. *J. Chem. Phys.* **1972**, *56*, 371.
(29) Shui, V. H.; Singh, P. I.; Kivel, B.; Bressel, E. R. *AIAA J.* **1979**, *17*, 1178.
(30) Rudnyi, E. B.; Vovk, O. M.; Kaibicheva, E. A.; Sidorov, L. N. *J. Chem. Thermodyn.* **1989**, *21*, 247.
(31) Walter, C. W.; Hertzler, C. F.; Devynck, P.; Smith, G. P.; Peterson, J. R. *J. Chem. Phys.* **1991**, *95*, 824.
(32) Stolcic, D.; Kim, Y. D.; Gantefor, G. *J. Chem. Phys.* **2004**, *120*, 5.
(33) Gunion, R. F.; Dixon-Warren, S. J.; Lineberger, W. C.; Morse, M. D. *J. Chem. Phys.* **1996**, *104*, 1765.
(34) Sievers, M. R.; Armentrout, P. B. *J. Phys. Chem. A* **1998**, *102*, 10754.
(35) (a) Wang, L. S.; Cheng, H. S.; Fan, J. *J. Chem. Phys.* **1995**, *102*, 9480. (b) Wang, L. S.; Wu, H. In *Advances in Metal and Semiconductor Clusters. IV. Cluster Materials*; Duncan, M. A., Ed.; JAI: Greenwich, CT, 1998; pp 299−343.
(36) (a) Dolg, M.; Wedig, U.; Stoll, H.; Preuss, H. *J. Chem. Phys.* **1987** *86*, 866. (b) Dolg, M. In *Modern Methods and Algorithms of Quantum Chemistry*; Grotendorst, J., Ed.; NIC Series 1; Julich Research Center: Julich, Germany, 2000. (c) Leininger, T.; Berning, A.; Nicklass, A.; Stoll, H.; Werner, H.-J. Flad, H.-J. *Chem. Phys.* **1997**, 217. (d) Kuchle, W.; Dolg, M.; Stoll, H.; Preuss, H. Pseudopotentials of the Stuttgart/Dresden Group, 1998 (Revision: Aug 11, 1998); http://www.theochem.uni-stuttgart.de/pseudopotentiale).
(37) Martin, J. M. L.; Sundermann, A. *J. Chem. Phys.* **2001**, *114*, 3408.
(38) Dunning, T. H., Jr. *J. Chem. Phys.* **1989**, *90*, 1007.
(39) Kendall, R. A.; Dunning, T. H., Jr.; Harrison, R. J. *J. Chem. Phys.* **1992**, *96*, 6796.
(40) Becke, A. D. *J. Chem. Phys.* **1993**, *98*, 5648.
(41) (a) Becke, A. D. *Phys. Rev. A* **1988**, *38*, 3098. (b) Perdew, J. P.; Wang, Y. *Phys. Rev. B.* **1991**, *45*, 13244.
(42) (a) Burke, K.; Perdew, J. P.; Wang, Y. In *Electronic Density Functional Theory: Recent Progress and New Directions;* Dobson, J. F., Vignale, G., Das, M. P., Eds.; Plenum: New York, 1998. (b) Perdew, J. P.; Wang, Y. *Phys. Rev. B* **1996**, *54*, 16533.
(43) (a) Sherrill, C. D.; Lee, M. S.; Head-Gordon, M. *Chem. Phys. Lett.* **1999**, *302*, 425. (b) Alcami, M.; Mo, O.; Yanez, M.; Cooper, I. L. *J. Chem. Phys.* **2000**, *112*, 6131. (c) Cohen, R. D.; Sherrill, C. D. *J. Chem. Phys.* **2001**, *114*, 8257.
(44) Casida, M. E.; Jamrski, C.; Casida, K. C.; Salahaub, D. R. *J. Chem. Phys.* **1998**, *108*, 4439.
(45) Tozer, D. J.; Handy, N. C. *J. Chem. Phys.* **1998**, *109*, 10180.

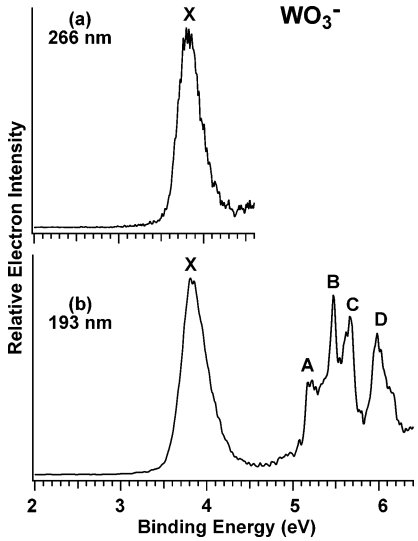

Figure 1. Photoelectron spectra of WO_3^- at (a) 266 nm (4.661 eV) and (b) 193 nm (6.424 eV).

occupied molecular orbital of the anion. All of the DFT calculations were carried out with Gaussian 03.[46]

We also did a set of calculations using the CCSD(T) method.[47] Geometries were optimized with the "aug-cc-pVDZ" for WO_3, WO_3^-, WO_4, and WO_4^-. For WO_5 and WO_5^-, we used the B3LYP geometries as described above. We also did calculations on WO_4 and WO_4^- with the B3LYP geometries. The CCSD(T) calculations were done starting from restricted Hartree−Fock wave functions for both the open- and closed-shell molecules. The closed-shell calculations were done with the RCCSD(T) approach, and the open-shell calculations were done with the UCCSD(T) approach. All of the coupled-cluster calculations were carried out using MOLPRO package.[48]

Experimental Results

WO_3^-. Photoelectron spectra of WO_3^- are shown in Figure 1. Only one band (X) was observed at 266 nm (Figure 1a) with discernible fine features. A VDE of 3.83 eV was obtained from the peak maximum. Since no well-resolved vibrational structures were obtained, the adiabatic detachment energy (ADE) was evaluated from the well-defined onset of band X by drawing a straight line at the leading edge of the band and then adding the instrumental resolution to the intersection with the binding energy axis. The ADE thus obtained was 3.62 ± 0.05 eV, which represents the electron affinity of neutral WO_3. The 193 nm spectrum (Figure 1b) revealed four additional bands at higher binding energies: A (5.22 eV), B (5.48 eV), C (5.68 eV), and D (5.98 eV). The observed ADE and VDEs for WO_3^- are collected in Table 1. The current 193 nm spectrum agrees with that by SKG; the higher binding energy features in the current data were slightly better resolved. SKG also presented a vibrationally resolved spectrum for the X band with a 30 meV spacing,[32] but they did not report ADE and VDE values for any spectral features.

Table 1. Observed Adiabatic (ADE) and Vertical (VDE) Detachment Energies for MO_n^- ($n = 3-5$) from Photoelectron Spectra (See Figures 1−3)[a]

obsd	ADE	VDE				
features	X	X	A	B	C	D
WO_3^-	3.62 (5)	3.83 (3)	5.22 (3)	5.48 (2)	5.68 (2)	5.98 (2)
WO_4^-	5.30 (5)	5.44 (3)	5.88 (2)	6.24 (2)		
WO_5^-	5.1 (1)	∼5.3	5.50 (3)	5.74 (2)	6.16 (2)	
MoO_3^-	3.135 (15)	3.33 (5)	5.13 (5)	5.35 (3)	5.63 (2)	
MoO_4^-	5.20 (7)	5.45 (5)	5.82 (2)	6.02 (3)		
MoO_5^-	5.10 (7)	5.40 (5)	5.70 (5)	5.93 (2)	6.20 (5)	

[a] All energies are in eV. Numbers in parentheses represent the experimental uncertainties in the last digits.

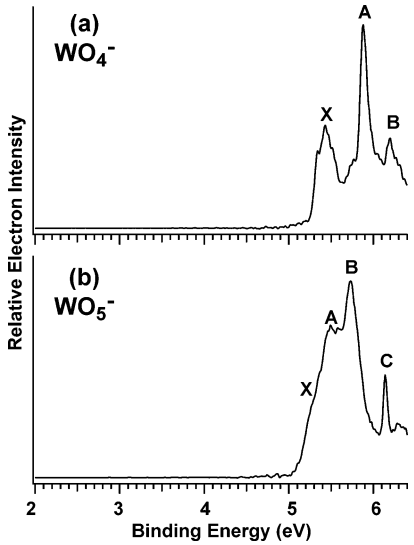

Figure 2. Photoelectron spectra of (a) WO_4^- and (b) WO_5^- at 193 nm (6.424 eV).

WO_4^-. In contrast to WO_3^-, WO_4^- possesses extremely high electron binding energies and only 193 nm photons could be used for photodetachment, as shown in Figures 2a. A complex spectrum was observed with three identifiable bands (X, A, and B). The lowest energy band (X) was broad with a reasonably sharp onset, which yielded an ADE of 5.30 eV. The band maximum gave a VDE of 5.44 eV for the ground-state transition. Band A with a VDE of 5.88 eV was intense and relatively sharp, but there seemed to be shoulders on both sides of band A. Band B at 6.24 eV was relatively weak. The observed ADE and VDEs for WO_4^- are also given in Table 1.

We specifically note that the current spectrum of WO_4^- is completely different from that reported previously by SKG.[32] SKG only presented a spectrum at 266 nm for WO_4^- that showed a single band with relatively poor signal-to-noise ratios in the binding energy range between 2 and 3 eV. We were unable to reproduce the SKG spectrum, despite extensive experimental efforts using different detachment photon energies and different source conditions. Our data suggested that a single 266 nm photon would not be sufficient to detach WO_4^-.

WO_5^-. WO_5^- also possesses very high electron binding energies. Its PES spectrum at 193 nm (Figure 2b) exhibited a broad, partially resolved band between ∼5.1 and 6 eV with a very sharp peak (C) at 6.16 eV. Three overlapping features may be tentatively identified within the broad band, X, A, and B, among which the B band at 5.74 eV was well defined. Band X appeared as a shoulder in the lower binding energy side, and

(46) Frisch, M. J. et al. *Gaussian 03,* Rev. B. 04; Gaussian, Inc.: Pittsburgh, PA, 2003.
(47) Watts, J. D.; Gauss, J.; Bartlett, R. J. *J. Chem. Phys.* **1993**, *98*, 8718.
(48) Werner, H.-J.; Knowles, P. J.; Amos, R. D.; Bernhardsson, A.; Berning, A.; Celani, P.; Cooper, D. L.; Deegan, M. J. O.; Dobbyn, A. J.; Eckert, F.; Hampel, C.; Hetzer, G.; Korona, T.; Lindh, R.; Lloyd, A. W.; McNicholas, S. J.; Manby, F. R.; Meyer, W.; Mura, M. E.; Nicklass, A.; Palmieri, P.; Pitzer, R. M.; Rauhut, G.; Schutz, M.; Stoll, H.; Stone, A. J.; Tarroni, R.; Thorsteinsson, T. *MOLPRO-2002, a package of ab initio programs;* Universitat Stuttgart and University of Birmingham: Stuttgart, Germany and Birmingham, U.K., 2002.

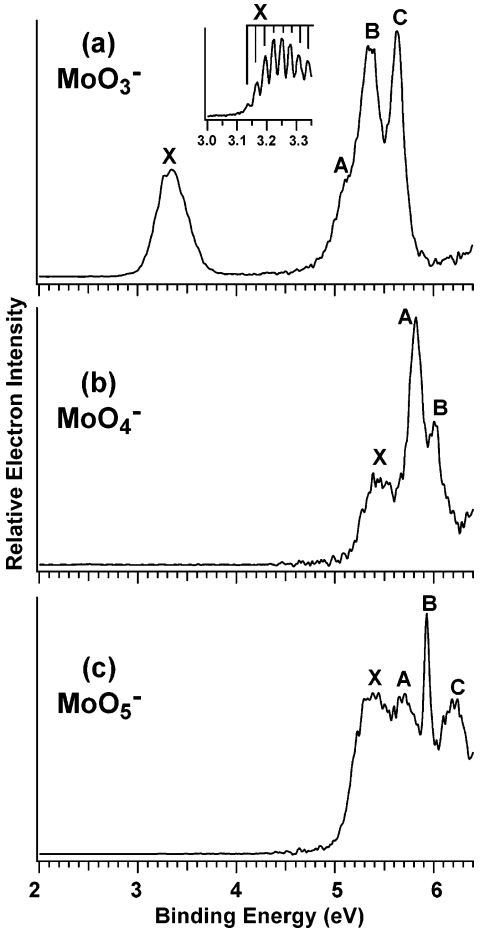

Figure 3. Photoelectron spectra of MoO_n^- ($n = 3-5$) at 193 nm (6.424 eV). The inset in a shows the spectrum of MoO_3^- at 355 nm with a well-resolved vibrational progression.

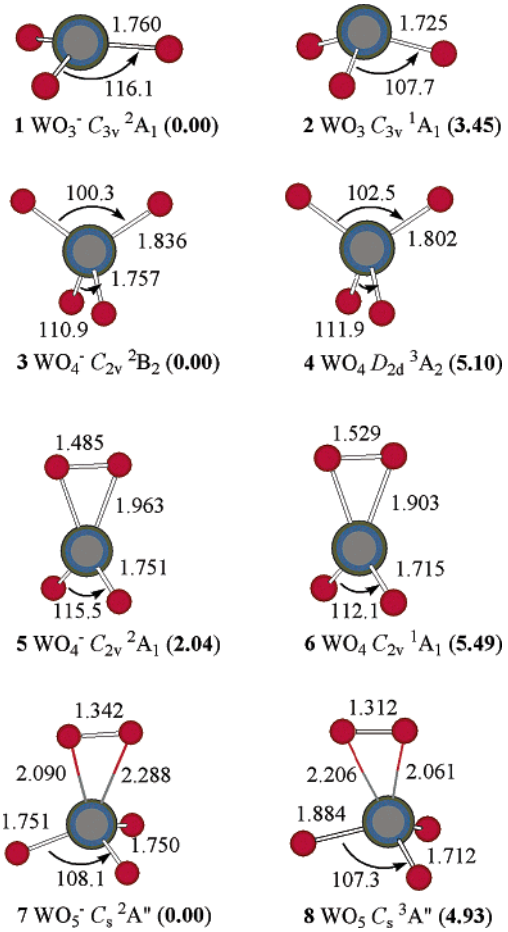

Figure 4. Optimized geometries for WO_n and WO_n^- ($n = 3-5$) at B3-LYP level of theory. Bond lengths are in Å, and bond angles are in degrees. The numbers in parentheses are energies in eV relative to the ground state of the anions.

an ADE of ~5.1 eV was estimated from the threshold. The ADE and VDEs for WO_5^- are also given in Table 1.

MoO_n^- ($n = 3-5$). Photoelectron spectra of MoO_n^- ($n = 3-5$) at 193 nm are shown in Figure 3. Very similar spectra were observed for the MoO_n^- species compared to those of WO_n^-. A vibrationally resolved spectrum with a spacing of 230 ± 30 cm^{-1} was obtained for the ground-state transition of MoO_3^- at 355 nm, as shown in the inset in Figure 3a. This vibrational spacing is similar to that observed by SKG for the ground-state band of WO_4^-.[32] In the 193 nm spectrum of MoO_3^-, a large energy gap was observed with three more bands appearing at higher binding energies (A, B, C). For MoO_4^- and MoO_5^- there is a one-to-one correspondence between the spectral features of the Mo and W clusters. All the observed ADEs and VDEs for MoO_n^- ($n = 3-5$) are given in Table 1, along with those for WO_n^-.

Computational Results

Optimized ground-state geometries of WO_3, WO_4, and WO_5 and their anions are presented in Figure 4, and those of a low-lying isomer of WO_4^- and WO_4 are also given. Theoretical ADEs and VDEs at the DFT and CCSD(T) levels are given in Table 2.

WO_3^- and WO_3. The ground state of WO_3^- (**1**) has C_{3v} symmetry with a $^2A_1$ electronic state. The W−O bond length, ∠OWO bond angle, and out-of-plane angle are 1.760 Å, 116.1°, and 11.8°, respectively, at the B3LYP level and 1.767 Å, 115.9°, and 11.8° at the aug-cc-pVTZ/CCSD(T) level. The planar D_{3h} structure is a transition state for inversion with a low out-of-plane imaginary vibrational mode (108.4i cm^{-1}) and a small barrier height (1.2 kcal/mol). The neutral WO_3 molecule (**2**) is

Table 2. B3-LYP and CCSD(T) Calculated Detachment Energies (eV) for WO_3^-, WO_4^-, and WO_5^-

		B3-LYP			CCSD(T)	
	detachment channel	ADE	VDE (α) (singlet)	VDE (β) (triplet)	ADE[a,b]	VDE[a]
WO_3^- [c]	$(7a_1)^{-1}$	3.45	3.83		3.37 (3.45)	3.67
	$(1a_2)^{-1}$		5.46	5.35		
	$(6e)^{-1}$		5.68	5.44		
	$(6a_1)^{-1}$		6.27	5.77		
	$(5e)^{-1}$		7.69	6.53		
WO_4^- [d]	$(6b_1)^{-1}$	5.22	5.69	5.66	5.11 (5.16)[e]	5.25[e]
	$(2a_2)^{-1}$		6.26	5.91		
	$(10a_1)^{-1}$		6.32	5.94		
	$(6b_2)^{-1}$		6.63	6.21		
WO_5^- [f]	$(9a'')^{-1}$	4.93	5.36	5.35		
	$(19a')^{-1}$		5.57	5.49		
	$(8a'')^{-1}$		5.69	5.69		
	$(18a')^{-1}$		6.13	5.92		
	$(17a')^{-1}$		6.47	6.44		

[a] At aug-cc-p-VTZ-CCSD(T) level. [b] Numbers in the parentheses at aug-cc-p-VDZ-CCSD(T) level. [c] The valent electronic configuration of WO_3^- is $6a_1^2 6e^4 1a_2^2$ $(7a_1^1)^\alpha$. [d] The valent electronic configuration of WO_4^- is $9a_1^2 4b_1^2 4b_2^2 1a_2^2 5b_2^1 5b_1^2 6b_2^2 10a_1^2 2a_2^2 6b_1^2$. [e] ADE and VDE of WO_4^- at the DFT geometry are 5.34 (5.17) and 5.51 eV, respectively. [f] The valent electronic configuration of WO_5^- is $16a'^2 6a''^2 7a''^1 17a'^2 18a'^2 8a''^2 19a'^2 9a''^2$.

closed shell ($^1A_1$) and also has C_{3v} symmetry. The lowest triplet state of WO_3 ($^3A_2$) is 1.71 eV higher in energy at the B3LYP level. The W−O bond length for neutral WO_3 (1.725 Å) [1.737 Å at the aug-cc-pVTZ/CCSD(T) level and 1.763 Å at the aug-cc-pVDZ/CCSD(T) level] is decreased by 0.03−0.04 Å as compared to the anion. Significant changes occur in the bond angles of neutral WO_3: the ∠OWO angle decreases to 107.7° at the B3LYP level (108.3° at CCSD(T)/aug-cc-pVTZ), which is near the tetrahedral bond angle, and the out-of-plane angle increases to 21.1° (20.6°, CCSD(T)/aug-cc-pVTZ), showing an increased pyramidalization at the central W site. Consistent with this change in geometry, the umbrella inversion of the neutral WO_3 at the B3LYP level has a much larger barrier (16.1 kcal/mol) than that of the corresponding anion. The W−O bond length in WO_3 at 1.72 Å is similar to a wide range of oxo bond lengths for oxo−tungsten compounds that we have calculated, consistent with a simple description of the bonding in this molecule as three W═O double bonds.

WO_4^- and WO_4. A range of isomers was studied in the search of the ground states for WO_4 and its anion. The two lowest energy isomers are given in Figure 4 (**3**−**6**). All methods agree that the ground state of WO_4^- was $^2B_2$ with C_{2v} symmetry, with the four oxygen atoms bonded to tungsten in a distorted tetrahedron (**3**). The distortion to C_{2v} symmetry from T_d symmetry leads to two kinds of oxygen atoms, two with longer bonds (1.836 Å) at the B3LYP level [1.868 Å at CCSD(T)/aug-cc-pVDZ], which we label as oxyl $(-O^{\bullet})^{-0.5}$ oxygens, and two as oxo (═O) oxygens with shorter bonds [1.757 Å at the B3LYP level; 1.789 Å at CCSD(T)/aug-cc-pVDZ]. The B3LYP ∠OWO bond angle between the oxyl oxygens shows significant deviation from the tetrahedral value, 100.3° at the B3LYP level [99.7° at CCSD(T)/aug-cc-pVDZ], whereas the ∠OWO bond angle between the oxo oxygens is near tetrahedral, 110.9° at the B3LYP level [111.3° at CCSD(T)/aug-cc-pVDZ]. The ground state of WO_4^- is well separated in energy (by 2.04 eV) from the second stable isomer with a di-oxygen (O−O) bond (**5**).

The calculation of the ground state of neutral WO_4 (**4**) was particularly difficult due to symmetry-breaking issues, which in part manifest themselves in very small HOMO−LUMO gaps. There are a number of possible geometries to consider for WO_4. In analogy to the anion, WO_4 can be described as either a distorted tetrahedral molecule or O_2 complexed to a bent WO_2. It is predicted to be a triplet derived from T_d symmetry and must distort due to the Jahn−Teller effect. The geometry at the B3LYP level converged to a symmetry-broken triplet (^3A) minima with C_1 symmetry. Whereas the triplet D_{2d} and C_{2v} structures for WO_4 were second-order stationary points, the triplet C_s structure was a first-order one leading to the C_1 minimum. The energy difference between all these structures was less than 0.03 eV. As mentioned earlier, B3LYP failed to yield the delocalized (D_{2d}) structure, which is a resonance hybrid of the two localized C_{2v} structures. This failure can be traced back to the mixing of HF-exchange in the functional.[43a]

Calculations by PW91xPW91c resulted in a D_{2d} ($^3A_2$) ground state for neutral WO_4 with delocalized W−O bonds (1.802 Å); no other minima were identified. In addition, other functionals without any HF exchange also yielded a D_{2d} minimum structure. Again, convergence of the wave function was hampered by the near degeneracy of the HOMO and LUMO orbitals. We also performed detailed calculations on WO_4 starting from the B3LYP geometries at the CCSD(T)/aug-cc-pVDZ level. The lowest energy structure was the D_{2d} triplet with a W−O distance of 1.828 Å and a ∠OWO bond angle of 102.2°, significantly distorted from the ideal T_d geometry. Of real interest is that the W−O bond distance is not that of an oxo O but is more like that of an oxyl (−O•). The other structures with lower symmetry were all higher in energy at the CCSD(T) level. Thus, we conclude that the ground state of WO_4 is $^3A_2$ with D_{2d} symmetry with the spin density shared on all four oxygen atoms.

Other possible isomers beyond those derived from T_d WO_4 are higher in energy. The neutral di-oxygen isomer (**6**) is 0.39 eV higher in energy than the ground state at the B3LYP level (Figure 4). Our optimized structures differ from the speculation by SKG,[32] who suggested that WO_4^- may have a peroxyl-type structure with only one oxygen in the O_2 moiety connected to W. We found no stationary point for a peroxyl structure, as all such initial structures at all DFT levels of theory collapsed to either the distorted T_d ground state or to the di-oxygen isomer on optimization.

WO_5^- and WO_5. An extensive search of the potential-energy surface of WO_5^- and WO_5 at the B3LYP level yielded only one di-oxygen type of stable structural arrangement (**7** and **8**). The ground state of WO_5^- ($^2A''$) and WO_5 ($^3A''$) can be viewed as O_2^- interacting with a WO_3 fragment and O_2^- interacting with a WO_3^+ fragment, respectively. The O_2^- is oriented parallel to one of the W−O bond vectors in both the neutral and the anion. Support for this description comes from the structural parameters. The O−O bond lengths in **7** and in **8** are 1.342 and 1.312 Å, respectively, very close to the O−O bond length in molecular O_2^- (1.352 Å) at the B3LYP level. The W−O bond lengths in the WO_3 fragment in WO_5^- are 1.750 and 1.751 Å, only slightly longer (0.025 Å) than the W−O bond length in WO_3 (1.725 Å). Correspondingly, the bond distances of the O_2 moiety to W in **7** are 2.090 and 2.288 Å, much longer than the W−O single bonds, which are in the range of 1.9 Å based on a large number of structures that we have calculated. No significant structural change in the O−O moiety was predicted on removal of an electron to form neutral WO_5 except for the slippage of the O_2 unit toward one of the oxo atoms (**8**). However, in the WO_3 moiety, one of the W−O bonds is significantly elongated (1.884 Å). This long bond is much longer than an oxo W═O bond and is very similar to that of a W−O single bond. This suggests a major electronic and structural reorganization upon electron detachment.

Discussion

Our discussion will mainly focus on the WO_n/WO_n^- series for which extensive theoretical calculations were carried out. The structures and bonding in MoO_n/MoO_n^- are expected to be similar to the W counterparts, as can be seen from their similar PES spectra.

Stoichiometric Molecule: WO_3. W has a $5d^46s^2$ valence electron configuration and forms a stoichiometric molecule with the three O atoms in WO_3, which is a stable gaseous species. However, the molecular properties of the WO_3 molecule are not well understood, and there is no definitive spectroscopic data about WO_3 in the gas phase. For example, the electron affinity of WO_3 was widely scattered in the literature.[27−31] The most recent review on atomic and molecular electron affinities[49]

lists a value of $3.33_{-0.15}^{+0.08}$ eV for WO_3 from a threshold photodetachment experiment.[31] In the work by SKG,[32] the electron affinity of WO_3 was not reported. Our photoelectron spectra yielded an ADE of 3.62 ± 0.05 eV for WO_3 determined from the detachment threshold of the 266 nm spectrum of WO_3^-. Provided that there is a measurable Franck−Condon factor for the 0−0 detachment transition, our measurement should represent an accurate electron affinity for WO_3.

The ground state of WO_3 was predicted to be closed shell ($^1A_1$, C_{3v}) with a valence electron configuration of $6a_1^2 6e^4 1a_2^2$, which are all primarily O 2p-type orbitals. The WO_3^- anion was predicted to be a doublet ($^2A_1$, C_{3v}) with the extra electron occupying the $7a_1$ LUMO of WO_3, giving rise to an electron configuration of $6a_1^2 6e^4 1a_2^2 7a_1^1$ for WO_3^-. The $7a_1$ MO is primarily a nonbonding d_z^2 orbital localized on W. Occupation of this MO induces a significant planarization in WO_3^- in which W is only slightly out of the plane defined by the three oxygen atoms whereas in the neutral molecule W is substantially more out-of-plane (Figure 4). There were no significant changes in the W−O bond length between WO_3 and WO_3^-. Therefore, on photodetachment from the anion, the inversion mode of the neutral is expected to be active. The ground-state detachment transition (X) of WO_3^- was indeed very broad, consistent with an unresolved vibrational progression of a low-frequency inversion mode. The calculated inversion mode frequency for WO_3 at the B3LYP level is 278 cm^{-1}, consistent with the vibrational spacing observed in the previous PES study of WO_3^- by SKG (30 meV or ~240 cm^{-1}).[32] In the current study we observed a broad vibrational progression with a spacing of 230 ± 30 cm^{-1} for the ground-state transition of MoO_3^- (Figure 3a). Similar to WO_3^-, this should be due to the inversion mode of C_{3v} MoO_3, which we calculated to be 284 cm^{-1} at the LDA level.

The second PES band in WO_3^- (A in Figure 1b) should correspond to the first triplet excited state of WO_3 due to removal of an electron from the $1a_2$ MO, i.e., the HOMO of neutral WO_3. The A−X energy difference represents an approximate experimental measure of the HOMO−LUMO gap for the neutral molecule. We measured a HOMO−LUMO gap of 1.4 eV for WO_3 and 1.8 eV for MoO_3. The calculated VDE for the ground-state transition of WO_3^- was 3.83 eV at the B3LYP level (Table 2), in excellent agreement with the experimental result. The CCSD(T)/aug/cc-pVTZ value for the VDE is 3.67 eV. The theoretical ADE for the ground-state transition at both B3LYP and CCSD(T) (Table 2) is also in reasonable agreement with the experimental measurement. Detachment from the fully occupied MOs will each lead to a triplet and singlet final state. The calculated VDEs for several valence MOs within our photon energy range are given in Table 2. Clearly, there are more detachment transitions in the higher binding energy side in the 193 nm spectrum of WO_3^- (Figure 1b) than were resolved. Overall, the calculated spectral pattern is in good agreement with the experimental PES spectra.

Diradical WO_4 and Delocalized Electrons. WO_4^-, as well as MoO_4^-, possesses extremely high binding energies, which can be accessed only at 193 nm. Thus, WO_4 and MoO_4 belong to the category of strong oxidizers called superhalogens.[50] We found that many O-rich transition-metal clusters possess such high electron binding energies, which is a consequence of delocalization of the extra electron over several O centers. The structure of the WO_4^- anion can be understood from the closed-shell tetrahedral WO_4^{2-} units, which exist in solids, such as Na_2WO_4. Removal of an electron from the T_d WO_4^{2-} results in a Jahn−Teller unstable WO_4^-, which distorts to a lower symmetry C_{2v} structure. All of the DFT functionals that we used gave similar results for the structure of WO_4^- as did the CCSD(T) method. The C_{2v} global minimum of WO_4^- was found to be well separated in energy from the second lowest energy isomer, which consists of a di-oxygen fragment and two W═O oxo units (**5** in Figure 4).

The ground state of WO_4^- anion is $^2B_2$ with a valence electronic configuration of $1a_2^2 5b_2^1 5b_1^2 6b_2^2 10a_1^2 2a_2^2 6b_1^2$ in the spin-unrestricted formalism. All these MOs are of O 2p type. Note that the unpaired spin is not in the HOMO. The negative charge in WO_4^- is delocalized over the two oxyl O atoms, significantly stabilizing the corresponding MO.

At the B3LYP level, the converged wave function showed that the first electron detachment is from the $6b_1^\beta$ orbital, giving a VDE of 5.66 eV, in reasonable agreement with the experimental value of 5.44 ± 0.03 eV. After orbital and geometry relaxation, we obtained a triplet ground state $^3A_1$ (D_{2d}) with delocalized W−O bonding for neutral WO_4, which is quite unusual and can be considered as a diradical. As shown in Table 2, the computed VDE values for transitions to other triplet neutral states are 5.91, 5.94, and 6.21 eV, whereas those for the singlet states are 5.69, 6.26, 6.32, and 6.63 eV. All of these transitions agreed well with the PES spectrum of WO_4^- (Figure 2a). Although only three bands are labeled, there are clearly more unresolved bands in the spectrum between the three main bands. At the CCSD(T)/aug-cc-pVTZ level, the VDE for the ground-state transition was calculated to be 5.25 eV using the calculated geometry at the CCSD(T)/aug-ccpVDZ level. The calculated VDE using the DFT geometry for WO_4^- is 5.51 eV. These results show that the calculated electron binding energies for this species are very sensitive to the geometry. The calculated ADE values are 5.22 eV at the B3LYP level and 5.11 eV at the CCSD(T)/aug-cc-pVTZ level (including PW91PW91 $\Delta ZPE = 0.29$ kcal/mol).

Our PES spectrum of WO_4^- differs completely from that reported recently by SKG.[32] The spectrum by SKG was taken at 266 nm, showing a single weak and broad band between 2 and 3 eV. The band appeared to have fine structures with a 180 meV spacing, but the signal-to-noise ratio of the spectrum was relatively low. The authors interpreted the 180 meV spacing as O−O vibration and concluded that there was "a transition from atomic-to-molecular adsorption of oxygen on tungsten atom" from WO_3 to WO_4. We made extensive efforts to reproduce the SKG spectrum, but we were not able to observe any photoemission signals at the low binding energy range (Figure 2a). We note that the $(O_2)WO_2^-$ species has been assigned from a matrix infrared spectroscopy study under cryogenic condition at 4 K.[24] Our calculations showed that such a species was much higher in energy (by 2.04 eV) than the global minimum structure (Figure 4). Thus, the $(O_2)WO_2^-$ isomer was unlikely to be populated in the cluster beam with

(49) Rienstra-Kiracofe, J. C.; Tschumper, G. S.; Schaefer, H. F., III; Nandi, S.; Ellison, G. B. *Chem. Rev.* **2002**, *102*, 231.

(50) (a) Gutsev, G. L.; Boldyrev, A. I. *Adv. Chem. Phys.* **1985**, *61*, 169. (b) Wang, X. B.; Ding, C. F.; Wang, L. S.; Boldyrev, A. I.; Simons, J. *J. Chem. Phys.* **1999**, *110*, 4763.

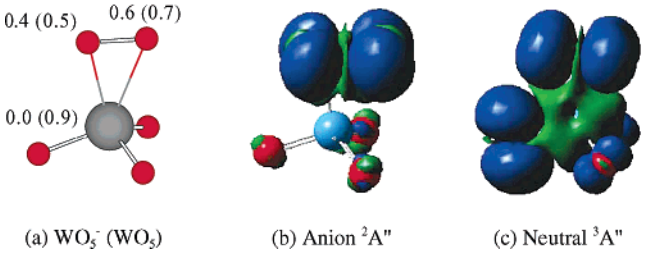

Figure 5. (a) Numerical spin densities of WO_5^- and WO_5 (in parentheses) in |e|. (b) Spin densities of WO_5^-. (c) Spin densities of WO_5. Blue represents the location of maximum spin density.

moderate supersonic cooling. Furthermore, the VDE of such an isomer was predicted to be 3.43 eV, which is much higher than that reported by SKG (~2.5 eV). Our spectrum showed no photoemission signals around 3.43 eV (Figure 2a), suggesting that the $(O_2)WO_2^-$ isomer was not populated in our experiment at any observable abundance, consistent with the fact that it is 2.04 eV higher in energy than the lowest global minimum WO_4^-. Our experimental and theoretical results suggested that the spectrum reported by SKG could not be due to the higher energy $(O_2)WO_2^-$ isomer of WO_4^-.

WO_5: Charge-Transfer Complex. The WO_5^- anion has C_s symmetry with an O−O moiety bonded to WO_3. It has a $^2A''$ ground electronic state with a valence electron configuration of $16a'^2 6a''^2 7a''^1 17a'^2 18a'^2 8a''^2 19a'^2 9a''^2$ in the spin-unrestricted formalism. Note that the excess spin does not arise from the HOMO. In fact, it is five orbitals below the HOMO (9a″), which is an oxygen lone pair. The structural parameters of WO_5^- (**7**, Figure 4) are consistent with a O_2^- unit interacting with a WO_3 fragment, $(O_2^-)WO_3$. This was borne out by the calculated spin density (Figure 5), which shows that the excess spin is almost completely localized on the O_2^- fragment. The orbital and geometry description of WO_5^- is clearly that of O_2^- bonded to WO_3.

The first calculated VDE (5.35 eV) at the B3LYP level arises from the $9a''^{\beta}$ orbital, in excellent agreement with the experimental VDE value of band X (5.3 eV, Figure 2b). This detachment channel removes an electron from the WO_3 fragment to form a distorted WO_3^+ and does not substantially perturb the O_2^- unit. As a result, in the neutral WO_5 except for the lateral shift of the O_2^- unit and a slight shortening of the O−O distance there were no major changes in the di-oxygen interaction with W. Consequently, neutral WO_5 can be described as O_2^- interacting with WO_3^+, essentially a charge-transfer complex, $(O_2^-)(WO_3^+)$. The spin density in WO_5 is consistent with the charge-transfer description, as shown in Figure 5c. One of the W−O bonds in the WO_3^+ fragment is considerably elongated in WO_5. This large geometrical change is consistent with the relatively broad ground-state detachment band observed for WO_5^- (X in Figure 2b). The calculated ADE at the B3LYP level for WO_5^- is 4.93 eV (Table 2), as compared to the experimental value of 5.1 ± 0.1 eV. The CCSD(T)/aug-cc-pVTZ ADE of 5.12 eV (including a ΔZPE(PW91PW91) of 0.40 kcal/mol) is in excellent agreement with the experimental value. The calculated VDEs from all the valence MOs within our photon energy are listed in Table 2. The overall theoretical VDE pattern agrees well with the PES spectrum.

Chemical Bonding in WO_n and WO_n^- (n = 3−5). The chemical bonding in the mono-tungsten oxide species can be understood conveniently using the valence-bond description as

Scheme 1. Valence-Bond Description of WO_n^- and WO_n (n = 3-5)

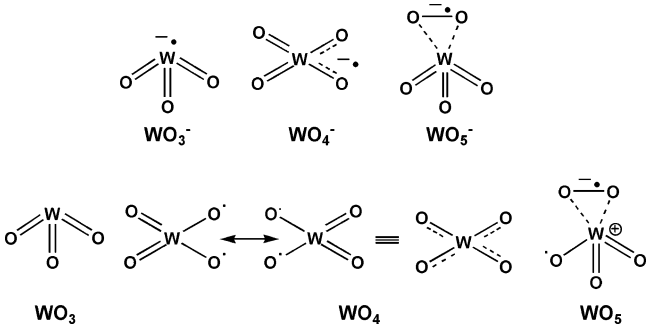

shown in Scheme 1. In WO_3 (C_{3v}) the six valence electrons of W form three W=O double bonds and a stable closed-shell molecule with a large HOMO−LUMO gap. In the anion the additional electron occupies the nonbonding d_z^2 orbital of W.

In neutral WO_4 the two unpaired electrons are completely delocalized over all four oxygen atoms. The D_{2d} ground state of WO_4 can be described as a resonance hybrid of two equivalent C_{2v} structures. Addition of an electron to WO_4 stabilizes the C_{2v} structure, leading to two W=O double bonds and delocalization of the extra charge over two O atoms. Whereas the short bonds can be described as being oxo bonds with 2c−2e dπ−pπ bonding, the long bonds can be described as two single W−O bonds resonantly stabilized by the additional electron in a π system just as that found in $-CO_2^-$. We calculated the energy for addition of O_2 to WO_2 to form WO_4 to be exothermic by 82.8 kcal/mol (3.59 eV) at the CCSD(T)/aug-cc-pVTZ level, indicating the formation of very strong W−O bonds. Taking the O_2 bond energy of 120 kcal/mol and assuming no change in the two original W−O bond energies and complete breaking of the O=O bond suggest that the average bond energy of the new W−O bonds is 102 kcal/mol. Addition of O_2^- to WO_2 can be estimated from our values and the electron affinity of O_2 (0.45 eV) to be highly exothermic by 194.7 kcal/mol or 8.44 eV [−3.59 + (−5.30) + 0.45]!

The chemical bonding in WO_5^- and WO_5 is very interesting and unexpected. The structure of WO_5^- shows that it is a complex formed by WO_3 and O_2^- fragments. The three short W=O bonds (1.751 Å) are only slightly elongated as compared to those in WO_3 (1.725 Å) (Figure 4), whereas the distances between O_2^- and W (2.090 and 2.288 Å) are much longer than those expected for W−O single bonds (1.90 Å). The O−O bond (1.342 Å) in WO_5^- was similar to that in free O_2^- (1.352 Å). In WO_5, one unpaired electron is localized on the O_2 fragment as in the case of the anion, and the other unpaired electron is localized on one of the O atoms of WO_3, giving rise to the unusual charge-transfer complex, $(O_2^-)WO_3^+$. We calculated the energy for addition of O_2 to WO_3 to form WO_5 to be exothermic by only 13.7 kcal/mol (0.59 eV) at the CCSD(T)/aug-cc-pVTZ level. This exothermicity is 3 eV less than that of WO_2 plus O_2 and shows that only a weak complex of O_2 with WO_3 is formed because the three oxo bonds in WO_3 have consumed all the available valency of W. In fact, the only way for O_2 to bind to WO_3 is for charge exchange to occur, leading to formation of a WO_3^+/O_2^- triplet charge-transfer complex. Addition of O_2^- to WO_3 occurs with a much higher exothermicity of 121.8 kcal/mol or 5.28 eV [−0.59 +(−5.14) + 0.45].

Comparison between WO_n and MoO_n. Both WO_4 and WO_5 and their anions are "oxygen-excessive" species. Superoxo-type ground-state structures might have been expected for such species, where the presence of an O−O bond could provide further stabilization. However, as clearly shown from our combined experimental and theoretical study, tungsten preferred tetrahedral coordination with oxygen in both WO_4 and WO_4^-, and no O−O bond was observed. In WO_5 two oxygen radical units, one $O^\bullet$ (from W−O) and one $O_2^{-\bullet}$, exist. For the WO_5^- anion the $O_2^{-\bullet}$ radical character is retained. Both WO_5 and WO_5^- may still be viewed as tetracoordinated if the O_2^- group is considered as a single species. The observations of oxygen radical character (W−$O^\bullet$ and $O_2^{-\bullet}$) and tetracoordinate tungsten in mono-tungsten oxide clusters are highly interesting and unexpected. Tetrahedral WO_4^{2-} species are stable structural units in bulk crystalline materials such as Na_2WO_4, $CaWO_4$, and $Al_2(WO_4)_3$.[51] Note that a W═O bond (160.6 kcal/mol, 6.96 eV) is much stronger than an O═O bond (119.1 kcal/mol, 5.17 eV),[52] which makes W═O bond formation energetically more favorable than O═O bond formation in WO_n and WO_n^-. For comparison, the MoO bond is 133.9 kcal/mol and the CrO bond is 102.6 kcal/mol.[52] The differences in bond energy may explain why the ground-state structure of CrO_4 is different from that of WO_4. CrO_4 possesses an O_2 unit,[17] whereas WO_4 preferred tetrahedral coordination with delocalized electrons. This is consistent with the fact that the Cr═O bond energy is less than that of O_2 whereas the opposite is true for W═O and O_2. As the bond energy for Mo═O is greater than that for O_2, we would expect MoO_4 to behave like WO_4 rather than CrO_4. The photoelectron spectra for MoO_n^- ($n = 3-5$) species show striking similarities to those of WO_n^-, but they were much different from those of CrO_n^-.[17]

Conclusions

A combined photoelectron spectroscopic and theoretical study was carried out on mono-tungsten and molybdenum oxide clusters MO_n^- (M = W, Mo; $n = 3-5$). Well-resolved PES spectral features were obtained and compared with theoretical calculations. A large energy gap was observed for the MO_3^- species between its low binding energy metal-d-based band and high binding energy oxygen-2p-based bands, characteristic of a stable closed-shell MO_3 neutral cluster. A dramatic increase in electron binding energies was observed between MO_3^- and MO_4^-: the ADEs measured for WO_3^- and MoO_3^- are 3.62 and 3.135 eV, respectively, and they increased to 5.30 and 5.20 eV for WO_4^- and MoO_4^-. The ADEs of the MO_5^- species are also extremely high, similar to those of the MO_4^- species. Only oxygen-2p-based detachment features were observed for MO_4^- and MO_5^-. Extensive electronic structure calculations at the density functional theory and CCSD(T) levels with large basis sets were performed on WO_n^- and WO_n ($n = 3-5$) to elucidate the electronic and structural evolution. WO_3^- and WO_3 were found to have C_{3v} structures with three oxo W═O bonds. A tetrahedral coordination environment about tungsten was found for WO_4 and WO_4^-: WO_4^- has C_{2v} symmetry with two W═O oxo units and the extra charge delocalized on the other two W−O units, whereas WO_4 has D_{2h} symmetry and two unpaired electrons each delocalized over two W−O units. WO_5^- can be viewed as an O_2^- interacting with a WO_3 unit, whereas neutral WO_5 is found to be a unprecedented charge-transfer complex, $(O_2^-)WO_3^+$. The observation of radical characters (W−$O^\bullet$ and $O_2^{-\bullet}$) in WO_4 and WO_5 may be relevant to the catalytic activity and selectivity of tungsten oxide catalysts.

Acknowledgment. We thank Dr. Jun Li for valuable discussions. This work was supported by the Chemical Sciences, Geosciences and Biosciences Division, Office of Basic Energy Sciences, U.S. Department of Energy (DOE), under grant no. DE-FG02-03ER15481 (catalysis center program) and was performed at the W. R. Wiley Environmental Molecular Sciences Laboratory, a national scientific user facility sponsored by DOE's Office of Biological and Environmental Research and located at Pacific Northwest National Laboratory, operated for DOE by Battelle.

JA046536S

(51) (a) Okada, K.; Morikawa, H.; Marumo, F.; Iwai, S. *Acta Crystallogr., Sect. B* **1974**, *30*, 1872. (b) Barker, A. S., Jr. *Phys. Rev. A* **1964**, *135*, 742. (c) Craig, D. C.; Stephenson, N. C. *Acta Crystallogr., Sect. B* **1968**, *24*, 1250.
(52) Kerr, J. A. In *CRC Handbook of Chemistry and Physics*; Lide, D. R., Ed., CRC Press: Boca Raton, FL, 2000.